Sensors and Materials, Vol. 36, No. 2 (2024) 427–442
MYU Tokyo

S & M 3529

A Simulation Model for a Blood Vessel Diameter Sensor

Tomohiro Kataoka,[1*] Takeshi Ando,[2] Noriko Tsuruoka,[3]
Ken Inaba,[2] and Yoichi Haga[1,3]

[1]Graduate School of Biomedical Engineering, Tohoku University,
Aza-Aoba, Aramaki, Aoba-ku, Sendai 980-8579, Japan
[2]Components BU, Origin Co., Ltd., Akatsuki, Oyama City, Tochigi 329-0211, Japan
[3]Graduate School of Engineering, Tohoku University, Aza-Aoba, Aramaki, Aoba-ku, Sendai 980-8579, Japan

(Received November 8, 2023; accepted January 9, 2024)

Keywords: blood pressure, blood vessel diameter, ultrasound, simulation, displacement

The development of cuffless blood pressure monitoring devices has been attracting attention in the field of medical devices. Measuring the diameter of blood vessels based on the A-mode waveform obtained by an ultrasound sensor attached to the body surface is suitable for daily blood pressure monitoring because of the simplicity of the device. However, movement by the user can cause device displacement, which reduces the received intensity of the wave reflected from the blood vessel wall, resulting in the incorrect measurement of the blood vessel diameter. To solve this problem, we previously proposed a blood vessel diameter sensor with an acoustic lens that transmits and receives ultrasound waves within a certain angular range along the long axis of the blood vessel, and verified the improved robustness of blood vessel diameter measurement compared with that with a planar sensor. The design of blood vessel diameter sensors requires the consideration of reflections and artifacts other than the blood vessel wall, and the use of simulation technology helps in efficient design. In this paper, we describe a simulation model for a blood vessel diameter sensor to support the design process. The simulation model was evaluated using an experimental blood vessel model (phantom) with characteristics similar to those for a human body, and the experimental and simulation results were found to be in agreement in terms of the angular range over which blood vessel diameters can be accurately measured and the effects of reflections and artifacts other than blood vessels. The simulation model is expected to accelerate our understanding of the effects of noise factors and the investigation of the causes of problems and improvements.

1. Introduction

1.1 Blood pressure measurement challenges

The ability to continuously or intermittently monitor blood pressure and detect sudden or periodic changes in blood pressure can generate new value.[1,2] Currently, blood pressure measurements in the medical field are carried out by compressing the upper arm or wrist with a

*Corresponding author: e-mail: tomohiro.kataoka@omron.com
https://doi.org/10.18494/SAM4771

ISSN 0914-4935
https://myukk.org/

cuff and measuring the blood pressure during decompression, which can cause discomfort for the user.[3,4] Therefore, this method is unsuitable for continuous/intermittent blood pressure monitoring without user awareness. Accordingly, cuffless devices have been developed for noninvasive and unconscious continuous/intermittent blood pressure monitoring.

Blood vessel diameter measurement using ultrasound is a cuffless method for blood pressure monitoring. An ultrasound transmitter/receiver is placed on the skin directly above the radial or carotid artery to detect waves reflected from the front and back walls of the blood vessel. The difference in arrival time between waves from the two walls is then used to determine the blood vessel diameter. However, because of individual differences in arterial stiffness and changes over time, calibration using a cuff blood pressure monitor is required when the blood vessel diameter sensor is installed. In addition, measurement with a cuff blood pressure monitor is also necessary in situations when absolute blood pressure accuracy is required. Nevertheless, ultrasound-derived blood vessel diameter waveforms have been reported to correlate with blood pressure waveforms, indicating the possibility of applying the ultrasound method to blood pressure monitoring.[5] The method can potentially predict the risk of cerebrovascular and cardiovascular events related to sudden blood pressure changes,[6] and may also provide valuable information that is different or complimentary to that obtained by conventional blood pressure measurement with pulse wave monitoring.[7] In particular, capturing reflections from the blood vessel walls as A-mode waveform peaks enables a simple system configuration and is expected to be applied to wearable devices.[8]

1.2 Effect of angular displacement between sensor and blood vessel

When measuring the blood vessel diameter using A-mode waveforms, a reduction in the output voltage associated with the reflected wave may result from the displacement of the sensor relative to the blood vessel caused by user body movement, or by the manner in which the device is worn, resulting in the incorrect measurement of the blood vessel diameter.[9] Previously, we experimentally studied the effect of the displacement between the sensor and the blood vessel on the measured blood vessel diameter.[10] We found that the angular displacement in the direction of blood flow (called long-axis displacement) has a significant effect on the robustness of the results obtained by the vessel diameter sensor. Conventional planar sensors are directional, and ultrasound waves are strongly transmitted in the direction normal to the sensor and only weakly in other directions. When the sensor and blood vessel are parallel [Fig. 1(a)], strong ultrasound waves are reflected in the normal direction from the blood vessel wall and return to the sensor. Thus, only normally reflected waves appear as peaks in the A-mode waveform. In contrast, when the sensor is not aligned in parallel with the blood vessel [Fig. 1(b)], the peak intensity decreases because the normally reflected waves do not necessarily return to the sensor, or those that do are superimposed out of phase. This makes the measurement of the blood vessel diameter more difficult.

To solve this problem, we previously proposed a blood vessel diameter sensor with an acoustic lens that transmits and receives ultrasound waves within a certain angular range in the long-axis direction (cylindrical lens, Fig. 2).[10] In this sensor, the ultrasound waves reflected in

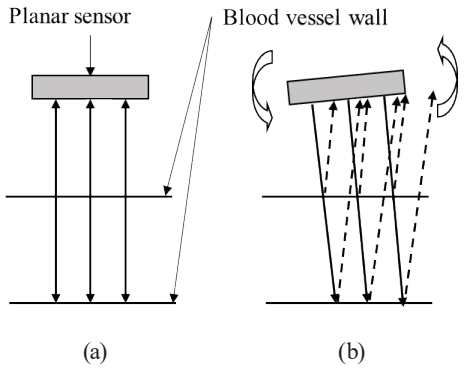

Fig. 1. Reflected ultrasound along long-axis direction for planar sensor. (a) Parallel alignment and (b) oblique alignment.

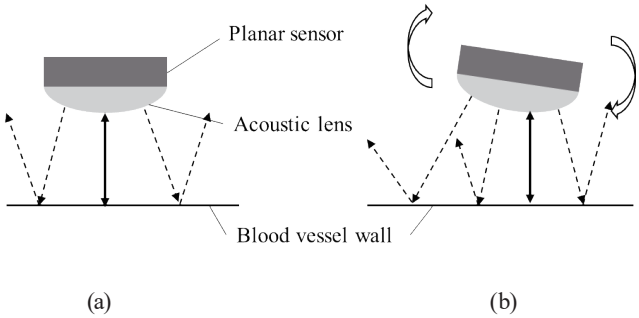

Fig. 2. Reflected ultrasound along long-axis direction for sensor with acoustic lens. (a) Parallel alignment and (b) oblique alignment.

the normal direction from the blood vessel wall are the most strongly received, even when the sensor and blood vessel are not aligned along the long-axis direction, thus giving measurement results similar to those in the case when the two are parallel. Furthermore, using a prototype sensor and a blood vessel model, we verified the robustness of blood vessel diameter measurement obtained by stabilizing the peak intensity of the blood vessel wall reflection even under angular displacement in the long-axis direction.[10]

In that investigation, we performed a comparison between a planar sensor and a sensor with an acoustic lens based on two criteria. Criterion A was the angular displacement range within which the peak intensity was maintained at ≥50% of its maximum value. This criterion is important because of competing contributions of reflections from structures other than the blood vessel wall. Criterion B was the angular range within which the error in the measured blood vessel diameter was within ±0.05 mm. As described in Sect. 1, the vessel blood diameter sensor is first calibrated using a cuff blood pressure monitor, so absolute accuracy is not required for blood vessel diameter measurements. The range ±0.05 mm (= 0.1 mm) corresponds to approximately half the wavelength of the transmitted ultrasound wave, and an error greater than this can indicate erroneous readings of waves reflected from the blood vessel wall.

1.3 Effect of lateral displacement between sensor and blood vessel

Although the proposed blood vessel diameter sensor with an acoustic lens can maintain the peak signal intensity over a wide angular range, it has the disadvantage of a lower output voltage than planar sensors. In addition, the ultrasound radiation angle must be optimized to minimize the effect of reflections other than those from the target blood vessel walls. Therefore, many prototypes and evaluations are required to optimize the design. Simulations are an effective means of reducing both the cost of prototyping and the length of the evaluation period.

In this paper, we present a simulation model for the proposed blood vessel diameter sensor to support its design. We then validated this model using an experimental blood vessel model (phantom) with properties similar to those for a human body.

2. Evaluation Model

The evaluation model used in this study was a model that we previously developed and evaluated in our research on ultrasound blood vessel diameter sensors.[10] These sensor and blood vessel models are described in the following sections. The sensor has an acoustic lens that radiates ultrasound waves in the long-axis direction. The blood vessel model (phantom) is a silicone resin tube with an inner diameter similar to that for a radial artery and is immersed in water. The phantom was used instead of a human blood vessel to compare the simulation and experimental results. In particular, the use of a phantom greatly reduces experimental uncertainty and also allows the angular displacement between the sensor and the blood vessel to be set arbitrarily during the evaluation. Although differences in acoustic properties with the human body affect the reflection intensity and angle, for this evaluation, it affects only the angle of travel of ultrasonic waves in the 0.5-mm-thick section of the tube and is not considered to affect the results.

2.1 Sensor

The sensor consists of a piezoelectric element, a backing, and an acoustic lens. The piezoelectric element is made of lead zirconate titanate (PZT; M material, Nippon Ceratec) with dimensions of 0.3 mm in the thickness direction, 5 mm in the short-axis direction, and 4 mm in the long-axis direction. Epoxy resin (EPO-TEK 301-1, Epoxy Technology) is mixed with tungsten powder (High Purity Chemical Laboratory; approximately 0.6 μm particle diameter) on the side opposite to the radiation surface and cured to make a backing. The frequency constant for the piezoelectric element in the thickness direction is 2050 Hz·m, and the sensor radiates ultrasound waves with a frequency of approximately 6.8 MHz. The acoustic lens is a cylindrical lens made from acrylic resin and has a circular arc in the long-axis direction only. It is bonded to the radiating surface of the piezoelectric element with UV-cured adhesive (UVA-6260K3, Resinus Kasei; Fig. 3).

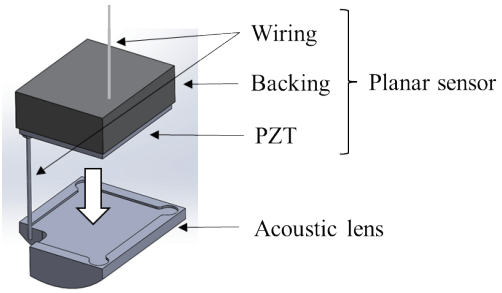

Fig. 3. (Color online) Structure of sensor with an acoustic lens.

2.2 Blood vessel model

A silicone resin tube with an inner diameter of 3 mm and an outer diameter of 4 mm is placed in a tank filled with water. The experimental equipment can be tilted in the long-axis direction up to an angle of ±10° while the sensor remains fixed (Fig. 4). The distance between the sensor and the tube is set to 6 mm. The inner diameter of the tube is set to 3 mm to correspond to the diameter of a typical radial artery. The distance of 6 mm between the sensor and the tube is larger than the actual radial artery depth, and is selected as such to suppress the ringing effects generated by the prototype sensor.

3. Simulation Model

3.1 Simulation tool (k-Wave)

The open-source k-Wave toolbox, which is widely used in fields such as photoacoustic tomography, was used as the simulation tool.[11] k-Wave can be used to set up a grid in the simulation domain, find values at grid points using interpolation methods, set up interpolation functions using appropriate basis functions, and calculate the spatial derivatives of variables on the grid. The simulation conditions are constructed with an interface that takes four parameters: kgrid (calculation grid), medium (propagation medium), source (sound source), and sensor (ultrasound detector).[12]

Because it runs in MATLAB, the feedback method for evaluation results and data analysis is simple and developable for analysis. Pressure values for each grid unit at each time step can be output, which enables the confirmation of the process over time. Furthermore, there are many examples of human body applications, and it is easy to obtain validated data for the human body and phantom media conditions. For these reasons, we have concluded that the system is suitable as a tool to support the design of blood vessel diameter sensors.

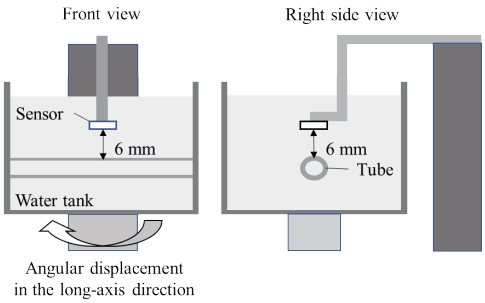

Fig. 4. (Color online) Blood vessel model.

3.2 Simulation model

The simulation was carried out on a two-dimensional planar model consisting of a *Y*–*Z* planar cross-sectional geometry of the evaluation model (Fig. 5). Because the evaluation model is symmetric in the *X*-direction, there were no major obstacles to verification, and the priority was to reduce the analysis time. The dimensions reflect the design values for the evaluation model, with the exception of the distance from the sensor to the tube (4.7 mm in the simulation model and 6 mm in the evaluation model). The conditions were designed to be similar to those for an actual radial artery.

3.3 Simulation conditions

3.3.1 Calculation grid

The simulation space is two-dimensional, with a computational grid resolution (spatial resolution) of 10 μm and an analysis area of 2048 × 2048 grid units (approximately 20 × 20 mm^2). In the simulation of a sensor with an acoustic lens with a radius of curvature of R6.0 mm (R6.0 mm lens), the same A-mode waveforms were obtained for spatial resolutions of 10 and 5 μm.

3.3.2 Propagation medium

The acoustic properties (sound velocity and density) of the constituent media in the simulation model are shown in Table 1. For the PZT, the density is that listed in the manufacturer's catalog. The sound velocities have typical values for common piezoelectric ceramics. The lens and tube were assigned sound velocities and densities typical of acrylic and silicone resins, respectively. The characteristic parameters for water at 25 °C were applied to the water in the tank.

The backing is composed of a composite material comprising epoxy mixed with tungsten powder, so typical values could not be applied. From a comparison of the A-mode waveforms of the simulation results with the experimental results for a planar sensor without a lens, a

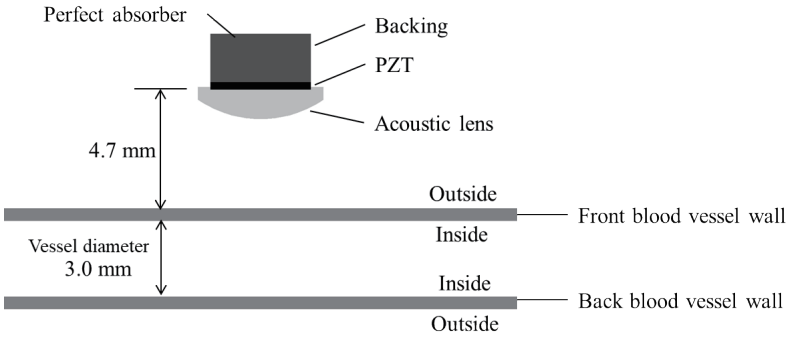

Fig. 5. Simulation model.

Table 1
Acoustic properties of simulation model.

Medium	Material	Sound velocity (m/s)	Density (kg/m^3)	Acoustic impedance ($Pa\ s/m^3$)
Backing	Composite of epoxy and tungsten	2700	5000	13500
PZT	PZT	4000	7700	30800
Lens	Acrylic	2730	1180	3221
Water	Water	1497	997	1429
Tube	Silicone resin	1000	997	997

reasonable value of acoustic impedance was found to lie in the range of 10000–15000 $Pa{\cdot}s/m^3$. On the basis of this result, the sound velocity was set to the typical value for the epoxy resin, and the density was set to 5000 kg/m^3. The backing material for the actual prototype is approximately 2 mm thick, but in the simulation, the backing was extended to the edge of the analysis area, with this edge modeled as a perfect absorber to eliminate the effects of reflection.

3.3.3 Sound source

The sound source was a single pulse of 6 MHz sine wave pressure applied to all grid units in the PZT using k-Wave's toneBurst command. In the experiment, a square pulse voltage was applied to the PZT, but the output ultrasound waveform was close to a sine wave. The applied intensity was set so that the peak of the pressure waveform was approximately 500 Pa.

3.3.4 Ultrasound detector

The sensor output intensity was calculated as the sum of the pressures received by all the grid units of the PZT. Initially, the pressure detected only by the surface layer of the PZT was used as the sensor output intensity. However, with this setup, the surface layer units repeatedly detect the pressure reflected within the PZT, resulting in ringing. Therefore, the sensor output intensity was set as the sum of the pressures received by all the grid units in the PZT.

4. Simulation Model Evaluation Methods

The simulation model was evaluated by comparing the simulation and experimental results for the angular dependence of the long-axis angular displacement. In this evaluation, we confirmed the effectiveness of using the simulation model for device design in terms of how to set the target radiation angle and whether design issues can be resolved and design improvements can be developed.

4.1 Selection of sensors with acoustic lenses to be evaluated

The maximum long-axis angular displacement between the sensor and the blood vessel was assumed to be approximately ±5° to ±10°. Therefore, we conducted simulations to estimate the required radius of curvature of the sensor acoustic lens to ensure the stable measurement of the blood vessel diameter in the angular range of ±5° to ±10°.

4.2 Simulation results

Simulations were performed at 1° intervals from 0 to 10°, and the blood vessel diameter was calculated from the A-mode waveform. Local maxima and minima were detected using the findpeaks function in MATLAB. Peaks were defined as the case where the difference between the local maximum and minimum values was the largest near the blood vessel wall. In the simulations, the separation limit for the local maximum obtained by the findpeaks function was set to 10 points. Peaks were regarded as brood vessel wall reflections, and the distance between the inside of the front blood vessel wall and that of the back blood vessel wall was calculated; this distance was defined as the blood vessel diameter (Fig. 6).

Four lens curvature radii were simulated: R4.0 mm, R4.5 mm, R5.0 mm, and R6.0 mm. Figure 7 shows the dependence of the peak intensity for the inside of the front blood vessel wall (front wall) and that of the back blood vessel wall (back wall) on the long-axis angular displacement. In the sensor with an R6.0 mm acoustic lens, the angular range in which a high peak intensity was maintained (peak intensity ≥50% of maximum value) was approximately 5°, but this range expanded for the R5.0 mm and R4.5 mm lenses, and was approximately 10° for the R4.0 mm lens. Similar results were obtained for the angular range within which the error in the measured blood vessel diameter was within ±0.05 mm.

4.3 Evaluation conditions for the experiment

In the experiment, evaluations were performed at 0.5° intervals from −10 to 10°. The number of points was larger that that for the simulation to compare the results for negative and positive angles and to assess the impact of measurement errors. The peak definition and detection method are the same as in the simulation, but the separation limit for the local maximum of the findpeaks function was set to 0.05 V.

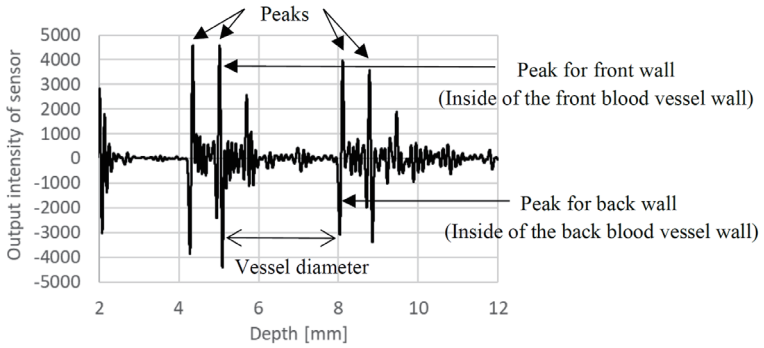

Fig. 6. Simulated A-mode waveforms (lens R4.5 mm, 0°).

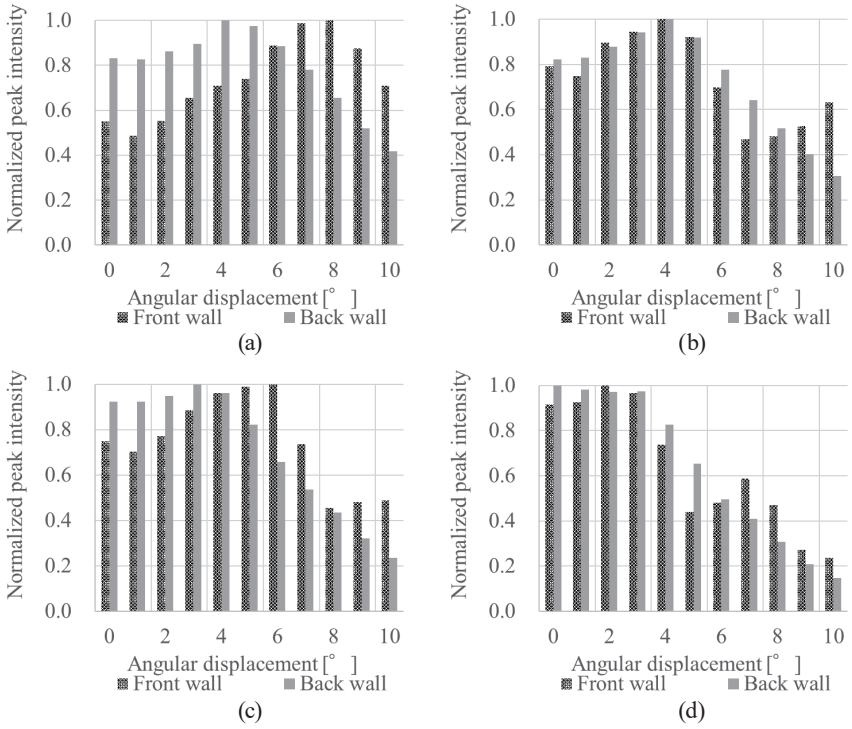

Fig. 7. Simulated dependence of peak intensity on angular displacement calculated by simulation. (a) R4.0 mm lens, (b) R4.5 mm lens, (c) R5.0 mm lens, and (d) R6.0 mm lens.

Ultrasound waves were generated by applying a voltage pulse of 100 μJ to the PZT using a pulser-receiver system (5800PR, Olympus). The waves reflected from the blood vessel wall were detected by the sensor, amplified by the pulser-receiver system (40 dB), and monitored by an oscilloscope to obtain A-mode waveforms, an example of which is shown in Fig. 8.

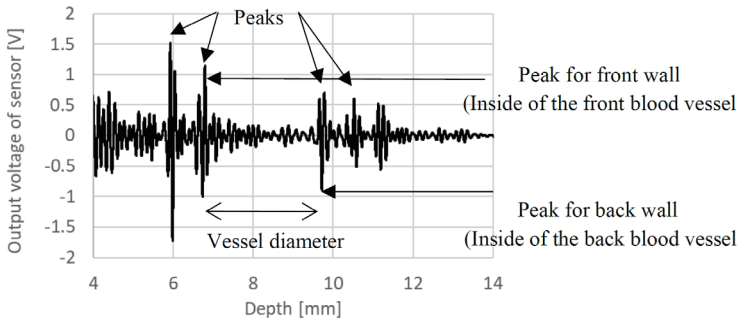

Fig. 8. Experimental A-mode waveform (lens R4.5 mm, 0°).

5. Evaluation Results

5.1 Comparison of simulation and experimental results

The simulation and experimental results for the peak intensity and vessel diameter are compared in Fig. 9 for four sensors with acoustic lenses of different radii as a function of the angular displacement. The peak intensities are normalized with respect to the maximum value over the entire angular range from −10 to 10°.

5.2 Comparison of angular ranges yielding only small variations in vessel diameter

Simulation and experimental results for the angular displacement range that yields stable blood vessel diameters are given in Table 2. The stability was evaluated on the basis of Criteria A and B defined in Sect. 1.2.

6. Discussion

6.1 Effectiveness of simulation model in designing angular displacement

In Fig. 9, it can be seen that the angular range where a high peak intensity is maintained increases as the lens curvature radius decreases. The same trend is observed for the angular range where the error in the vessel diameter becomes larger than ±0.05 mm. The R6.0 mm lens cannot obtain accurate results for an angular range larger than 5°, but as the lens curvature radius decreases, the angular range for accurate measurements increases to about 6–7° for R5.0 mm, about 7–8° for R4.5 mm, and about 10° for R4.0 mm. When used as a wearable device, the maximum long-axis angular displacement between the sensor and the blood vessel is assumed to be about 5–10°, so a lens with about R4.0 mm is suitable on the basis of the results obtained here.

In Table 2, the experimental and simulation results are seen to be in generally good agreement for all lens curvatures. This demonstrates that the simulation model is capable of estimating the long-axis angular range over which the vessel diameter can be measured.

Fig. 9. Simulation and experimental results for peak intensity and blood vessel diameter plotted against angular displacement in the long-axis direction. Results are for sensors with acoustic lenses with four different radii. (a) R4.0 mm lens, (b) R4.5 mm lens, (c) R5.0 mm lens, and (d) R6.0 mm lens.

Table 2
Long-axis angular displacement range for stable vessel diameter measurement.
Criterion A: peak intensity higher than 50% of maximum peak
Criterion B: error of measured vessel diameter within ±0.05 mm

Criterion			Simulation	Experiment
R4.0	Criterion A	Front side	Angular range 20.0° (−10 to +10°)	Angular range 16.5° (−10 to −8°, −5.5 to +4.5°, +5.5 to +10°)
		Back side	Angular range 18.0° (−9 to +9°)	Angular range 18.0° (−10 to −9.5°, −8.5 to +9.0°)
	Criterion B		Angular range 20.0° (−10.0 to +10.0°)	Angular range 18.5° (−10 to −7.0°, −5.5 to +10.0°)
R4.5	Criterion A	Front side	Angular range 14.0° (−10.0 to +9.0°, −6 to +6°, +9 to +10°)	Angular range 14.0° (−8.0 to −7.5°, −6.5 to +7.0°)
		Back side	Angular range 16.0° (−8.0 to +8.0°)	Angular range 15.0° (−7.5 to +7.5°)
	Criterion B		Angular range 14.0° (−10.0 to −9.0°, −6 to +6°, +9 to +10°)	Angular range 17.0° (−9.0 to −7.5°, −9.5 to +10.0°)
R5.0	Criterion A	Front side	Angular range 14.0° (−7.0 to +7.0°)	Angular range 13.0° (−10.0 to −8.0°, −4.0 to +4.0°, +5.5 to +8.5°)
		Back side	Angular range 14.0° (−7.0 to +7.0°)	Angular range 12.5° (−6.5 to +6.0°)
	Criterion B		Angular range 14.0° (−7.0 to +7.0°)	Angular range 15.5° (−5.5 to +10.0°)
R6.0	Criterion A	Front side	Angular range 8.0° (−4.0 to +4.0°)	Angular range 10.0° (−5.0 to +5.0°)
		Back side	Angular range 10.0° (−5.0 to +5.0°)	Angular range 10.0° (−5.0 to +5.0°)
	Criterion B		Angular range 12.0° (−6.0 to +6.0°, −4.0 to +4.0°, +6.0 to +8.0°)	Angular range 11.5° (−9.0 to −8.5°, −7.5 to +7.0°, −5.0 to +5.5°)

However, for some angular ranges, there is disagreement between the simulation and experimental results with regard to the peak intensity and blood vessel diameter. This is described in more detail below.

6.2 Correlation between simulation and experimental results

The peak intensity tends to decrease with increasing angular displacement for all lens curvatures. However, a dip and subsequent rise in peak intensity occurs in the angular range of 2–3° in both the simulation and experimental results. The dip appears only for the front blood vessel wall. In the simulation, it occurred between 7.0 and 8.0° for the R4.5 mm lens and between 5.0 and 6.0° for the R6.0 mm lens, whereas in the experimental results, it occurred between −7.5 and −5.5° and between 4.0 and 6.0° for the R4.0 mm lens, and between −7.5 and −5.5° and between 4.0 and 6.0° for the R5.0 mm lens. In these angular ranges, the normal reflection intensity of the front vessel wall decreased, and reflections from other angles and artifacts were detected as peaks. As a result, the vessel diameter could not be measured correctly.

To quantitatively evaluate the correlation between the simulation and experimental results, a correlation diagram of the angular characteristics of the peak intensity is shown in Fig. 10, and the corresponding correlation coefficients are given in Table 3. The correlation was calculated between the peak intensity values obtained in the simulation and experiment for given angular displacement values.

Although the back wall showed a high correlation of 0.8 or more for all lens curvatures, the correlation for the front wall was low for the R4.0 mm and R5.0 mm lenses. The reason for this low correlation is the dip in peak intensity that appears in the experimental results. On the other hand, the reason why the correlation coefficient does not decrease for the R4.5 mm and R6.0 mm lenses, where a dip appears in the simulation results, is that the size of the dip is smaller than in the experimental results. The cause of this difference is discussed in Sect. 6.3.

6.3 Causes of dip in peak intensity

Figures. 11 and 12 show the simulated and experimental A-mode waveforms, respectively, at angles near where the dip in intensity occurs. Figures. 11(a) and 12(a) show waveforms outside the dip, and Figs. 11(b) and 12(b) show those inside the dip. The second peaks (reflection by the inside of the front vessel wall) in Figs. 11(b) and 12(b) are smaller than their counterparts in Figs. 11(a) and 12(a). As a result, an artifact that is 0.7 mm deeper is detected as a peak, and the blood vessel wall distance is misread. To investigate the cause of the dip in the second peak intensity in Figs. 11(b) and 12(b), movies of the pressure intensity distribution output from the simulation were used to check ultrasound propagation. The following events were observed in the movies. There was a second reflected wave whose arrival time at the PZT was similar to that for the wave reflected by the inside of the front blood vessel wall, which was the measurement target. This second wave was reflected by the outer side of the blood vessel anterior wall after multiple reflections inside the lens [Fig. 13(a)]. These two reflected waves interfered within the PZT, causing a decrease in the second peak intensity. Fig. 13(b) shows the pressure intensity distribution at the moment when the ultrasound wave reflected from the inside of the front wall reached the PZT in the A-mode waveform (angle of 7°) shown in Fig. 11(b). As can be seen, positive and negative pressures were simultaneously present in the PZT, causing interference.

As to why the size of the dip in the simulation results was smaller than in the experimental results, consider the following: in the simulation, the ratio of the inside reflection intensity of the front blood vessel wall [(1) and artifact] to the outside reflection intensity [(2)] was higher than the experimental results, so the second peaks and the artifact were larger than the experimental results. As a result, the size of the dip in the simulation results was small, which does not affect the correlation coefficients. The difference in the ratio of the inside reflection intensity to the outside reflection intensity between the simulation and experimental results is due to the lower reflectance of the vessel wall in the simulation results than in the experimental results. The reflectance of the simulation can be made closer to the experimental results by optimizing the setting of the boundary conditions of the vessel wall.

The outside walls of blood vessels in the human body have acoustic properties similar to those of the surrounding tissues and therefore minimally reflect ultrasonic waves. Therefore, the

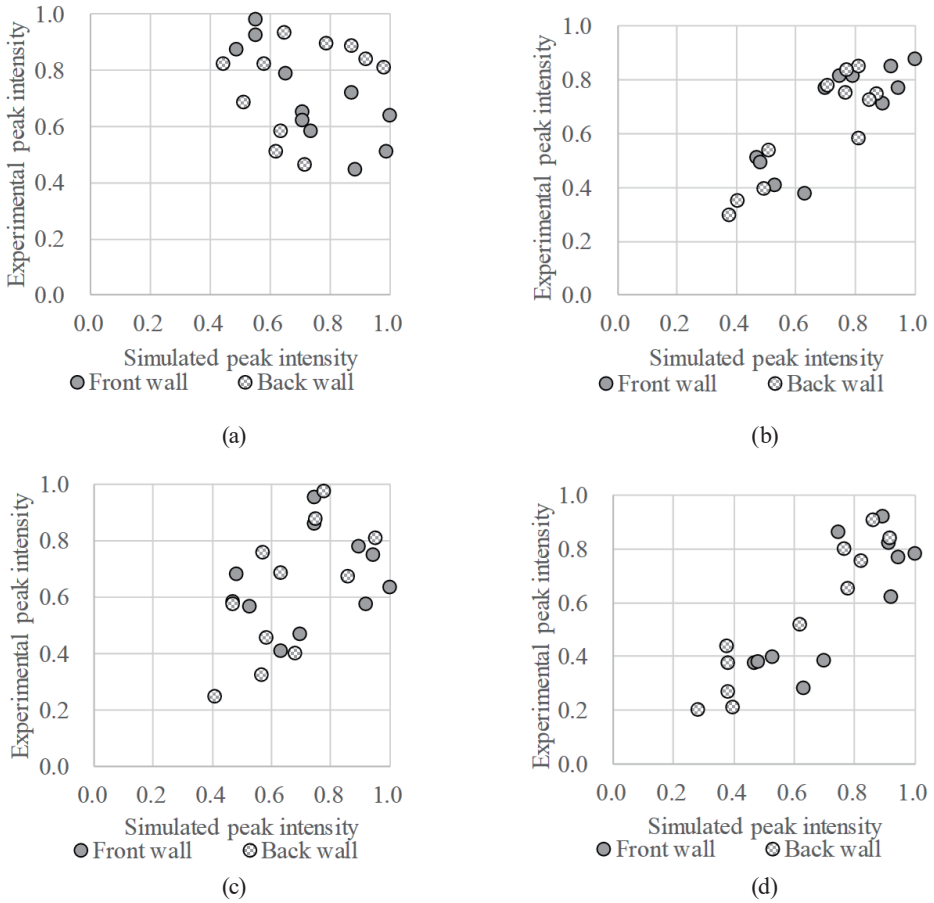

Fig. 10. Correlation diagrams for the simulation and experimental results for peak intensity for different angular displacements. Each data point represents a different angular displacement. (a) R4.0 mm lens, (b) R4.5 mm lens, (c) R5.0 mm lens, and (d) R6.0 mm lens.

Table 3
Coefficient of correlation between simulated and experimental peak intensities for different angular displacements.

	Front wall	Back wall
R4.0 mm	−0.79	0.93
R4.5 mm	0.82	0.92
R5.0 mm	0.28	0.90
R6.0 mm	0.80	0.83

above interference and dip in the peak angular characteristic are not expected to be reproduced in the human body. However, the human body contains reflectors other than blood vessels. The analysis of the effects of reflected waves and artifacts other than blood vessels by simulation would provide an understanding of the effects of noise factors and help improve sensor design.

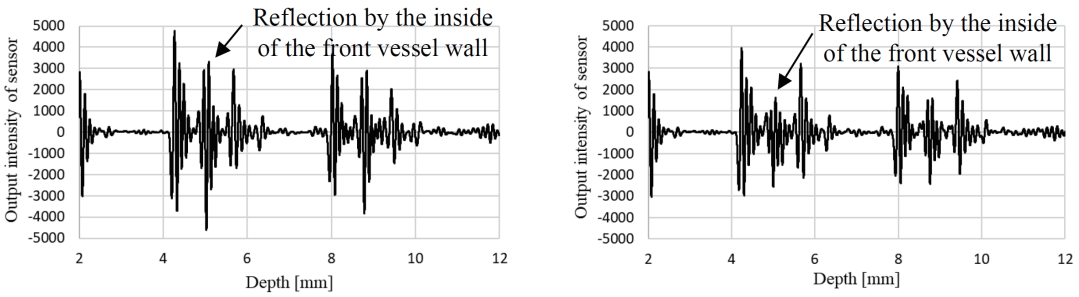

(a) (b)

Fig. 11. Simulated A-mode waveforms at angles near the occurrence of intensity dip. (a) R4.5 mm lens, 6° and (b) R4.5 mm lens, 7°.

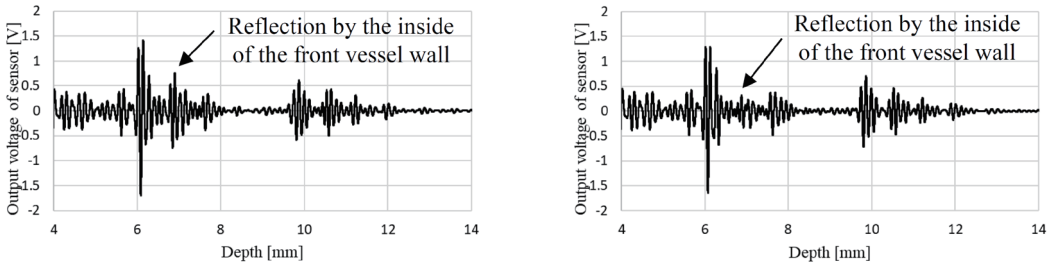

(a) (b)

Fig. 12. Experimental A-mode waveforms at angles near the occurrence of intensity dip. (a) R4.0 mm lens, −5° and (b) R4.0 mm lens, −6°.

(1) Ultrasound reflected from inside of front blood vessel wall (target of vessel diameter measurement)
(2) Ultrasound reflected from outside of front vessel wall after multiple reflections in the lens

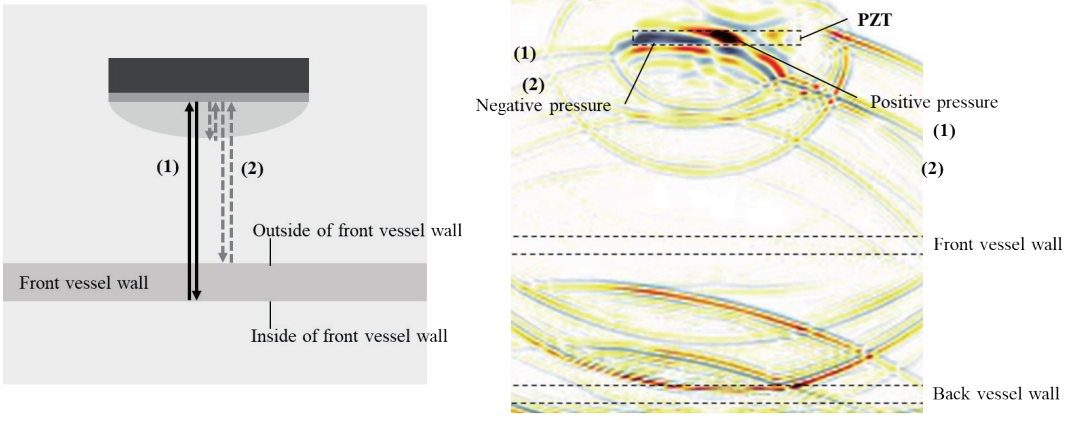

(a) (b)

Fig. 13. (Color online) Interference of two reflected waves causing the depression phenomenon. (a) Paths of two reflected waves and (b) pressure intensity distribution when the wave reflected by the inside of the front wall reached the PZT [Fig. 11(b)].

7. Conclusions

A simulation model of an ultrasound blood vessel diameter sensor was evaluated by comparing the simulation and experimental results for the effects of the long-axis angular displacement of the sensor. The simulation model can support the design of the sensor with regard to setting the angular range over which vessel diameters can be measured and investigating the causes of design problems and creating improvement plans.

However, the simulation could not reproduce the angular range in which a peak-intensity dip occurs in the experimental results. One reason is that the simulation model does not accurately reflect the experimental model. The PZT and lens models only reflect the design dimensions, not the actual dimensions. In addition, the simulation model does not include the thickness of the adhesive between the sensor and the lens. Because a quarter-wavelength is approximately 0.1 mm for the lens, we believe that it is necessary to reproduce the actual dimensions in the simulation model with at least the same accuracy. The effectiveness of design support through simulation can be further enhanced by matching the dimensions of the experimental and simulation models, including the blood vessel model.

By combining this simulation method with a human biological simulation model from previous studies, the design of a blood vessel diameter sensor that incorporates factors affected by reflections other than those from the vessel wall and artifacts can proceed without prototyping. As a result, this simulation approach is expected to accelerate the development of highly robust blood vessel diameter sensors and enable the realization of cuffless devices for noninvasive and unconscious continuous/intermittent blood pressure monitoring.

References

1 K. Kario, T. G. Pickering, T. Matsuo, S. Hoshide, J. E. Schwartz, and K. Shimada: Hypertension **38** (2001) 852. https://doi.org/10.1161/hy1001.092640
2 K. Kario, T. G. Pickering, Y. Umeda, S. Hoshide, Y. Hoshide, M. Morinari, M. Murata, T. Kuroda, J. E. Schwartz, and K. Shimada: Circulation **107** (2003) 1401. https://doi.org/10.1161/01.CIR.0000056521.67546.AA
3 P. Verdecchia, F. Angeli, C. Borgioni, R. Gattobigio, and G. Reboldi: Hypertension **49** (2007) 777. https://doi.org/10.1161/01.HYP.0000258215.26755.20
4 P. B. Bottini, R. B. Rhoades, A. A. Carr, and L. M. Prisant: Am. J. Hypertens. **4** (1991) 288. https://doi.org/10.1093/ajh/4.3.288
5 C. Wang, X. Li, H. Hu, L. Zhang, Z. Huang, M. Lin, Z. Zhang, Z. Yin, B. Huang, H. Gong, S. Bhaskaran, Y. Gu, M. Makihata, Y. Guo, Y. Lei1, Y. Chen, C. Wang, Y. Li, T. Zhang, Z. Chen, A. P. Pisano, L. Zhang, Q. Zhou, and S. Xu: Nat. Biomed. Eng. **2** (2018) 687. https://doi.org/10.1038/s41551-018-0287-x
6 K. Kario: Prog. Cardiovasc. Dis. **59** (2016) 262. https://doi.org/10.1016/j.pcad.2016.04.001
7 K. Takazawa: J. Tokyo Med. Univ. **75** (2017) 19 (in Japanese). https://tmu.repo.nii.ac.jp/?action=repository_action_common_download&item_id=11969&item_no=1&attribute_id=22&file_no=1
8 H. Hu, X. Zhu, C. Wang, L. Zhang, X. Li, S. Lee, Z. Huang, R. Chen, Z. Chen, C. Wang, Y. Gu, Y. Chen, Y. Lei, T. Zhang, N. H. Kim, Y. Guo, Y. Teng, W. Zhou, Y. Li, A. Nomoto, S. Sternini, Q. Zhou, M. Pharr, F. L. Scalea, and S. Xu1: Sci. Adv. **4** (2018). https://doi.org/10.1126/sciadv.aar3979
9 Y. Haga, K. Okuda, N. Tsuruoka, T. Suzuki, K. Fujita, T. Matsunaga, D. Kawakubo, and K. Maehira: IEEJ Trans. Sens. Micromachines **140** (2020) 265 (in Japanese). https://doi.org/10.1541/ieejsmas.140.265
10 T. Kataoka, T. Ando, N. Tsuruoka, K. Inaba, Y. Haga: Trans. Jpn. Soc. Med. Biol. Eng. **62** (2024) (in Japanese).
11 J. Jaros, E. Martin, and B. E. Treeby: IEEE Trans. Ultrason. Ferroelectr. Freq. Control. **67** (2020) 81. https://doi.org/10.1109/TUFFC.2019.2941795
12 X. Song, J. Wei, J. Xiong, and L. Song: Mul-ti-pulse Photoacoustic Microscopy Based on k-space Pseudospectral Method: Simulation Study (arXiv:2009) 00689. https://arxiv.org/abs/2009.00689